Hodell, D.A., Abrantes, F., Alvarez Zarikian, C.A., and the Expedition 397 Scientists
Proceedings of the International Ocean Discovery Program Volume 397
publications.iodp.org

Data report: X-ray fluorescence core scanning and revised composite section of Pliocene–Pleistocene sediments from IODP Expedition 397 Site U1587[1]

Carlos A. Alvarez Zarikian,[2] Timothy D. Herbert,[2] David A. Hodell,[2] Jerry F. McManus,[2] Lucien Nana Yobo,[2] Montserrat Alonso-Garcia,[3] José-Abel Flores,[2] Huai-Hsuan May Huang,[2] Lauren Haygood,[4] Myriam Kars,[5] Jesse Yeon,[6] Fatima Abrantes,[2] and the Expedition 397 Scientists[2]

[1] Alvarez Zarikian, C.A., Herbert, T.D., Hodell, D.A., McManus, J.F., Nana Yobo, L., Alonso-Garcia, M., Flores, J.-A., Huang, H.-H.M., Haygood, L., Kars, M., Yeon, J., Abrantes, F., and the Expedition 397 Scientists, 2026. Data report: X-ray fluorescence core scanning and revised composite section of Pliocene–Pleistocene sediments from IODP Expedition 397 Site U1587. In Hodell, D.A., Abrantes, F., Alvarez Zarikian, C.A., and the Expedition 397 Scientists, Iberian Margin Paleoclimate. Proceedings of the International Ocean Discovery Program, 397: College Station, TX (International Ocean Discovery Program). https://doi.org/10.14379/iodp.proc.397.203.2026

[2] **Expedition 397 Scientists' affiliations.** Correspondence author: **cazarikian@tamu.edu**
[3] Department of Geology, University of Salamanca, Spain.
[4] Boone Pickens School of Geology, Oklahoma State University, USA.
[5] International Ocean Drilling Programme, University of Plymouth, UK.
[6] Gulf Coast Repository, Texas A&M University, USA.

Keywords
International Ocean Discovery Program, IODP, *JOIDES Resolution*, Expedition 397, Iberian Margin Paleoclimate, Site U1587, X-ray fluorescence, XRF core scanning, Pleistocene, Pliocene

References (RIS)

MS 397-203
Received 20 May 2025
Accepted 15 January 2026
Published 18 February 2026

Abstract

During International Ocean Discovery Program (IODP) Expedition 397, four sites (U1586, U1587, U1385, and U1588) were drilled on a bathymetric transect across a submarine plateau on the Portuguese continental slope to intersect each major subsurface water mass of the eastern North Atlantic. Site U1587 (37°34.867′N, 10°21.531′W; water depth = 3479 m), the second deepest site along the depth transect and the second most distal from the coastline, was cored for reconstructing changes in physical and chemical properties of the deep eastern North Atlantic on short and long timescales. At this site, coring in three holes recovered 1566 m of sediment from which a continuous 595 m composite sequence of late Miocene to Holocene sediments was developed. The dominant lithologies are nannofossil ooze and clay in varying proportions that were accumulated at an average rate of 10 cm/ky. The high sedimentation rates and expanded section will permit the development of proxy records for high-resolution climate reconstruction spanning the past 7.8 My.

Following Expedition 397, the archive halves of the cores used to develop the shipboard composite depth scale of Site U1587 were analyzed using an Avaatech X-ray fluorescence (XRF) core scanner in the Gulf Coast Repository at Texas A&M University (USA) to obtain semiquantitative chemical elemental data at 1 cm resolution. In this report, we present the measured elemental records and the refined composite depth scale (splice) for the Pliocene and Quaternary sections at the site and provide a regression equation for estimating $CaCO_3$ weight percent by using the log(Ca/Ti) values.

1. Introduction

Site U1587 (37°34.8667′N, 10°21.5306′W; 3479 meters below sea level [mbsl]) was the second deepest site drilled during International Ocean Discovery Program (IODP) Expedition 397 in 2022 on a southwest bathymetric transect across the Promontório dos Príncipes de Avis (Figure **F1**), an elevated submarine plateau on the Portuguese continental slope that is isolated from the influence of turbidites (**Hodell et al.**, 2024b). Today, the site is bathed by a mixture of approximately 75% North Atlantic Deep Water (NADW) and 25% Lower Deep Water (LDW) originating from the Southern Ocean (Jenkins et al., 2015). However, the relative contributions of these water masses—

and their vertical distribution in the water column—have varied over time, with important implications for deep Atlantic Ocean circulation, ventilation, and carbon storage (**Hodell et al.**, 2024b).

Site U1587 was strategically selected to recover an expanded and continuous sedimentary sequence spanning the late Miocene to the Quaternary, enabling the investigation of multiple Expedition 397 objectives that include the evolution of millennial climate variability, orbital forcing of glacial–interglacial cycles, cyclostratigraphic patterns, the warm climate of the Pliocene, and the impact of the Messinian Salinity Crisis (**Hodell et al.**, 2024b). Three holes were cored at Site U1587: Hole U1587A was cored to 500 m core depth below seafloor, Method A (CSF-A), Hole U1587B was cored to 547.8 m CSF-A, and Hole U1587C was cored to 567.9 m CSF-A (Figure **F2**) using the R/V *JOIDES Resolution* advanced piston corer (APC) and extended core barrel (XCB) drilling systems (**Abrantes et al.**, 2024; **Hodell et al.**, 2024b). Coring in three holes recovered 1566 m of sediment from which a continuous 595 m composite sequence was developed following standard IODP procedures. These consisted of using Correlator software (version 4.0.1) to align correlative features in sediment physical properties (i.e., color reflectance parameter L*, magnetic susceptibility [MS], and the blue channel from the red-green-blue [RGB] light spectra extracted from the core section color images) between individual cores from all three holes (**Abrantes et al.**, 2024). This procedure shifts a core's CSF-A depth to a core composite depth below seafloor (CCSF) depth scale. The depth shifts for each core are used to define the composite spliced section by selecting and combining continuous sections of cores from multiple holes to form a complete stratigraphic representation at Site U1587 (**Hodell et al.**, 2024b).

The dominant lithologies at Site U1587 are nannofossil ooze and clay in varying proportions. Nannofossils are extraordinarily abundant, and foraminifers and ostracods are also common and generally well preserved; however, calcareous microfossil preservation and the proportions of benthic forms decrease with depth, and clay content increases. A robust biostratigraphy and magnetostratigraphy developed during Expedition 397 indicate a continuous and complete sequence from the late Miocene (Tortonian; 7.8 Ma) to the Holocene with a sediment accumulation rate averaging 10 cm/ky (**Hodell et al.**, 2024b). The high sedimentation rates and the expanded, well-preserved stratigraphic section will permit the development of proxy records for high-resolution paleoceanographic and paleoclimatic reconstructions at millennial timescales spanning the past 7.8 My. This will allow researchers to track climate system evolution from the warm Pliocene through the intensification of Northern Hemisphere Glaciation (NHG) in the late Pliocene, the obliquity-driven "41-kyr world," the mid-Pleistocene transition, and ultimately into the eccentricity-paced glacial cycles of the "100-kyr world" (**Hodell et al.**, 2024a; Hodell et al., in press).

Postexpedition X-ray fluorescence (XRF) core scanning of all four Expedition 397 sites (U1586, U1587, U1385, and U1588) was carried out at four different XRF laboratories to acquire nonde-

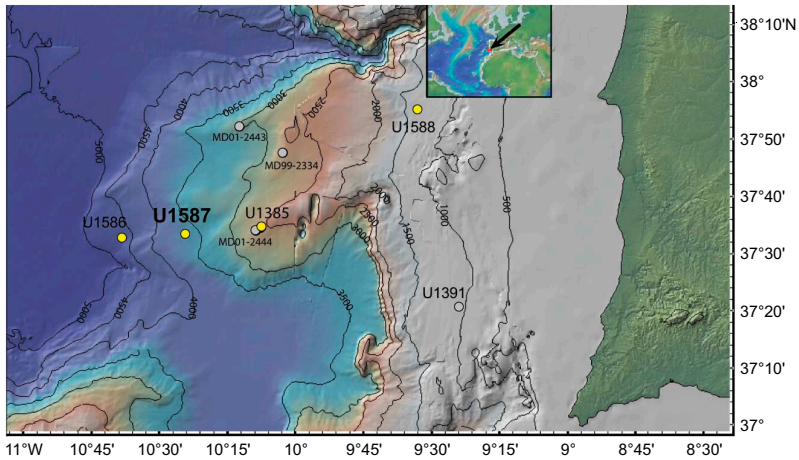

Figure F1. Bathymetry of Promontório dos Príncipes de Avis west of the Iberian Margin showing locations of Expedition 397 sites, Marion Dufrense (MD) piston cores, and Integrated Ocean Drilling Program Site U1391. Site U1385 was occupied previously during Expedition 339, as was Site U1391. Map modified from Hodell et al. (2024b, 2026).

structive, high-resolution semiquantitative records of major and minor elements and use them alongside existing physical properties data to refine the composite depth scales of each site. XRF measurements of Site U1587 (this report) were performed at the Gulf Coast Core Repository at Texas A&M University (USA). Site U1385 cores were measured at the Godwin Laboratory at the University of Cambridge (UK) (**Hodell et al.**, 2026). Site U1586 cores were measured at the EMSO-GOLD laboratories of the Divisão de Geologia e Georecursos Marinhos of Portuguese Institute for Sea and Atmosphere (IPMA) (Portugal) (**Abrantes et al.**, 2025). XRF measurements of Site U1588 cores were in progress at the Bremen Core Repository (Germany) at the time of publication of this report. In addition, IODP Expedition 401 returned to Site U1385 in 2024 and deepened it to 552.5 meters below seafloor (mbsf) to recover late Miocene to early Pliocene deposits (Flecker et al., 2024). Expedition 401 Site U1385 cores were XRF scanned at the Gulf Coast Repository (Raad et al., 2026).

Variations of major and minor elements through time can be related to past changes in Earth and ocean processes that affect the composition of the sediment and can be used for detailed paleoceanographic and paleoclimatological studies (Peterson et al., 2000; Bahr et al., 2014; Hodell et al., 2015; Seki et al., 2019; Wu et al., 2020; Lamy et al., 2024).

This report provides (1) the high-resolution XRF data for the Pliocene and Quaternary sections at Site U1587, (2) the refined affine and stratigraphic correlation (splice) tables, and (3) a regression equation for estimating the $CaCO_3$ weight percent by means of the log(Ca/Ti) values.

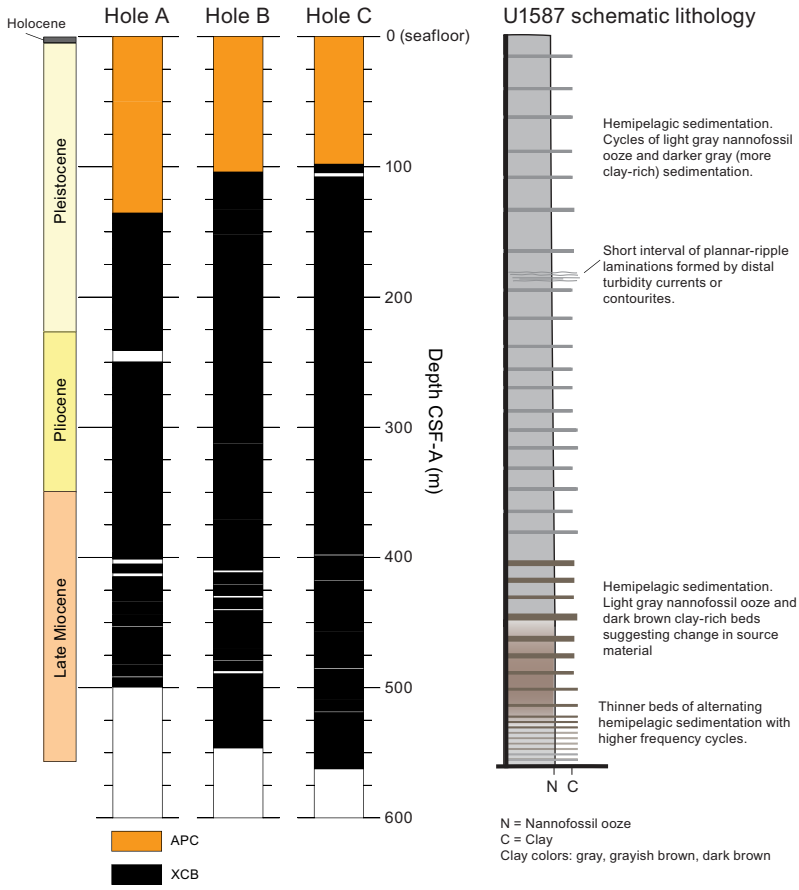

Figure F2. Core recovery, Holes U1587A–U1587C. White intervals = cores with no or incomplete recovery (see Abrantes et al. [2024] for details). Left: age boundaries of recovered sedimentary section based on the shipboard biostratigraphic and paleomagnetic boundaries. Right: schematic lithology across all holes. Dominant lithologies: nannofossil ooze (light gray) and clay (dark gray and brown) in varying proportions (see text and Hodell et al. [2024b] for details).

2. Materials and methods

2.1. X-ray fluorescence scanning strategy and data set structure

XRF core scanning of Site U1587 was conducted using the two Avaatech XRF core scanners (XRF1 and XRF2) at the Gulf Coast Core Repository under a programmatically allocated time window of 60 days from February to April 2023. Given the time constraint, a targeted scanning strategy was implemented to maximize data quality and coverage. Specifically, rather than every core section collected at the site, only the cores included in the shipboard splice (see Table **T31** in Hodell et al. [2024b]) were selected for scanning. Cores were scanned at two energy settings, 10 kV for light elements (e.g., Al, Si, S, K, Ca, Ti, and Fe) and 30 kV for heavier elements (e.g., Sr, Br, Zr, and Rb), to capture a representative geochemical profile of the site's sediment sequence. Some off-splice sections located near questionable splice tie points (see Gaps in **Hodell et al.** [2024b]) were also measured. The cores spanning the Pleistocene and Holocene stratigraphic section of the splice interval in each hole (Cores 397-U1587A-2H through 25X, 397-U1587B-4H through 25X, and 397-U1587C-1H through 24X) were measured on the XRF2 scanner, and the cores spanning the late Miocene through Pliocene section of the splice interval (Cores 397-U1587A-26X through 53X, 397-U1587B-28X through 59X, and 397-U1587C-26X through 61X) were measured on the XRF1 scanner.

The primary objective was to generate a high-resolution, continuous elemental record spanning the late Miocene through the Quaternary, enabling detailed paleoenvironmental and paleoceanographic reconstructions. However, the 2 month scanning window proved insufficient to complete the full measurement campaign, particularly given the length of the recovered section and the need for high-resolution (1 cm) measurements. To address this limitation, additional scanning time was arranged beyond the programmatic window extending through fall 2023 and external resources and technical support were allocated to complete the measurements.

As a result, the XRF data set for Site U1587 is divided into two components: a programmatic data set that includes the Pliocene and Pleistocene intervals, scanned during the original 60 day window and made publicly available through this report and IODP archives, and a proprietary data set that encompasses the late Miocene through the Pliocene transition, scanned during the extended measurement period and currently retained for ongoing research and analysis prior to public release. This two-part structure ensures continuity in the elemental record while supporting both immediate research objectives and future data sharing. This manuscript only presents the programmatic scanning data set and only discusses the methods for that data set.

2.2. XRF measurements

Before scanning, each core was removed from cold (4°C), humidity-controlled storage and allowed to equilibrate to room temperature. Allowing the cores to warm up to room temperature prevents condensation, which can affect X-ray attenuation (Tjallingii et al., 2007). The surface was then carefully cleaned by scraping across the core using a clean glass slide, ensuring that no material was displaced vertically, thereby preserving stratigraphic integrity. Finally, the cleaned surface was covered with a 4 μm thick Ultralene plastic film to prevent contamination of the measuring prism during scanning (Richter et al., 2006).

XRF data were collected every centimeter, with measuring locations occasionally shifted to avoid protruding clasts, cracks, and depressions along the core surface. Two scans at different voltages (10 and 30 kV) were completed for each core section measured. The 10 kV scan measured Mg, Al, Si, P, S, Cl, Ar, K, Ca, Ti, Cr, Mn, and Fe using a tube current of 160 μA, no filter, and a detection time of 10 s. The 30 kV scan measured K, Ca, Ti, Mn, Fe, Ni, Cu, Zn, Ga, As, Br, Rb, Sr, Y, Zr, Nb, and Mo using a tube current of 1250 μA, a Pd thick filter, and a detection time of 11 s. For all measurements, the sample irradiation area was 10 mm in the downcore direction and 12 mm in the cross-core direction. Further information on the analytical capabilities of the XRF Core Scanning Laboratory at the Gulf Coast Repository can be found at **https://sites.google.com/tamu.edu/gcr-xrf-core-scanning/home**.

Elemental intensities were derived by postprocessing the XRF spectra using bAxilbatch software, applying default spectrum-fitting models and standard processing parameters. The intensity of the elements depends on the elemental abundance and matrix effects within the window parameters, physical properties, the sample geometry, and the measuring prism of the scanner (Tjallingii et al., 2007). The clean XRF data are provided as counts per second.

The log ratio of Ca/Ti determined by XRF scanning was chosen as the basis for fine tuning and in some cases slightly revising the original shipboard splice because it is a high-quality proxy for the lithologic cycles of carbonate content (Hodell et al., 2015) that are so evident in shipboard descriptions and multisensor track (MST) data (e.g., MS, natural gamma radiation [NGR], and L*). Although Ca and Ti are measured simultaneously at both 10 and 30 kV, the 10 kV counts are significantly greater than those at 30 kV and are therefore considered to have a higher signal-to-noise ratio because the elemental signal is stronger relative to instrumental and background noise.

The log(Ca/Ti) is well correlated with 125 measurements of weight percent (wt%) $CaCO_3$ made by coulometric titration during Expedition 397 (**Abrantes et al.**, 2024; **Hodell et al.**, 2026), with a Pearson correlation coefficient (r) of 0.985 (Figure **F3**). The following regression equation allows estimation of $CaCO_3$ content from the Site U1587 XRF data and can be used, for example, to calculate carbonate accumulation rates (Hodell et al., 2013):

$$\text{wt\% } CaCO_3 = 40.245 \times \log(\text{Ca/Ti}) - 26.178.$$

2.3. Quality control

To ensure consistent data quality throughout the XRF core scanning process, instrument specific calibration standards were measured at a 9 kV excitation level at the start and end of each scanning day. Each morning, 20 replicate measurements were performed at each energy level to warm up and stabilize the instrument. In the evening, the standards were remeasured (without replicates), and the results were compared to the morning values to detect and correct for any instrumental drift over the course of the day(s).

Core deformation, fracturing, uneven surface, and the presence of coarse sedimentary clasts can compromise the contact between the XRF scanner sensor and the core surface. As part of the data quality assurance protocol, scan steps exhibiting positive argon (Ar) counts, indicative of ambient air detection resulting from inadequate sensor/core contact (Croudace and Rothwell, 2015), were systematically identified and excluded from the data set to maintain analytical reliability. Core sec-

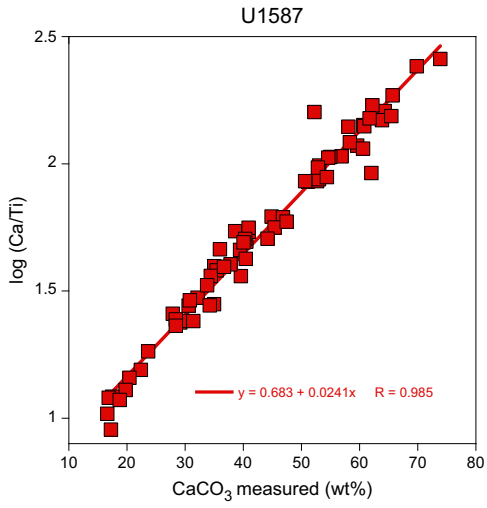

Figure F3. Comparison of $CaCO_3$ weight percentage measured by coulometric titration on 125 discrete sediment samples during Expedition 397 (Hodell et al., 2024b) and XRF-derived log(Ca/Ti) values at corresponding core depths, Site U1587. High variance ($R^2 = 0.97$) shows how well linear model fits data and supports use of log(Ca/Ti) as a proxy for $CaCO_3$ content.

tions in which 10% or more of scan steps registered positive Ar counts underwent visual inspection, reconditioning, and subsequent rescanning.

2.4. Stratigraphic correlation

The log ratio of Ca/Ti determined by XRF scanning was chosen as the basis for fine tuning and in some cases slightly revising the original shipboard splice because it is a high-quality proxy for the lithologic cycles of carbonate content (Hodell et al., 2015) that are so evident in shipboard descriptions and MST data (e.g., MS, NGR, and L*). Where possible, splice tie points followed shifts between holes downsection based on the shipboard composite, which primarily relied on MS data. However, tie points were occasionally adjusted by a few decimeters to take advantage of the more precise identification of local maxima and minima of correlative points provided by centimeter-scale XRF measurements.

To improve the precision and confidence of correlating these features, the log Ca/Ti records were smoothed using a Gaussian process (GP) filter from the GPy Python library (**https://gpy.readthedocs.io/en/deploy/GPy.core.html**) with a Matern32 kernel. This approach allowed tie points to be refined to just a few centimeters. Comparing this GP-smoothed Ca/Ti data with GP-treated L* data from the same composite interval (Figure **F4**) demonstrates the superior correlation precision of the XRF data. The higher signal-to-noise ratio of the XRF data is evident in the tighter fit to the primary data. The dispersion of the measured L* parameter (color reflectance; a proxy for carbonate content [Balsam et al., 1999]) relative to the GP fit is substantially larger than for the scan-

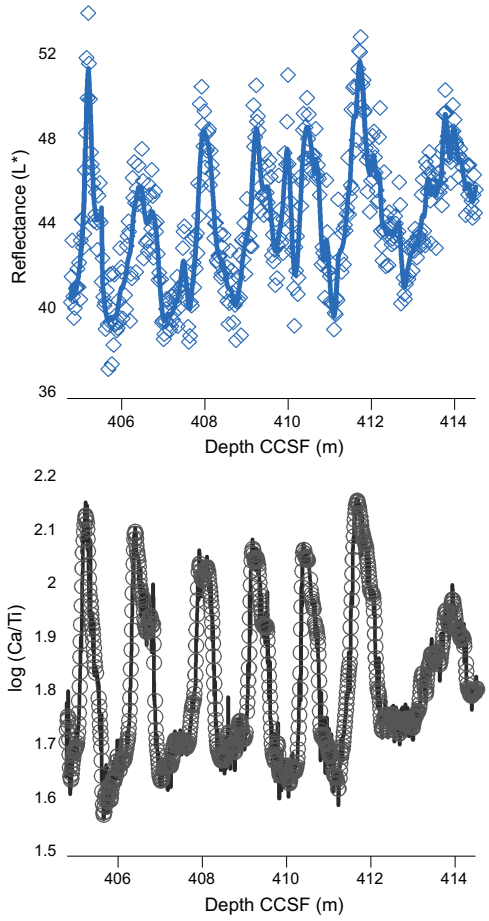

Figure F4. GP modeling of two nondestructive measurements of same cored interval along Site U1587 splice. Symbols = raw measurements. lines = GP fits to data. Note that dispersion of measured L* parameter (color reflectance; proxy for carbonate content [Balsam et al., 1999]) to GP fit is much larger than for scanning XRF measurement of log(Ca/Ti). GP fit explains less of the total variance in L* (92.5%) than in log(Ca/Ti) (98.4%), indicating greater signal-to-noise in XRF in comparison to L* measurements. See text for details.

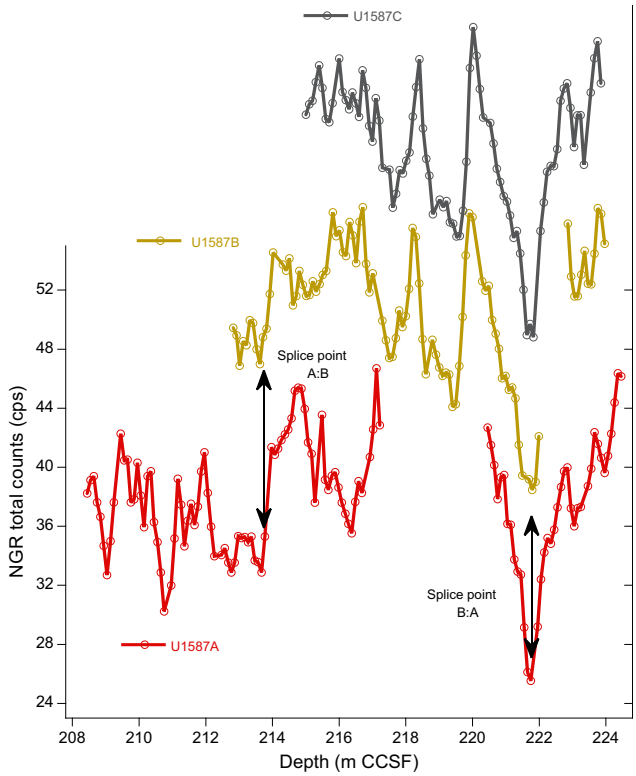

Figure F5. Revised splice using NGR to tie Holes U1587A and U1587B to fill gap in XRF scanning. Arrows = tie point for revised splice from Holes U1587A to U1587B and from Holes U1587B to U1587A. All hole segments aligned to composite depth scale. cps = counts per second.

ning XRF log Ca/Ti record. Here, variance refers to the proportion of total data variability explained by the GP model. The GP explains 92.5% of the variance in L*, compared to 98.4% for log Ca/Ti, indicating that the L* record contains a larger noise component and thus a lower signal-to-noise ratio. These results are consistent with broader assessments comparing XRF to other high-resolution proxies such as MS and L* for correlation purposes (e.g., **Abrantes et al.**, 2025; **Hodell et al.**, 2026).

XRF scanning identified one error greater than a decimeter relative to the shipboard splice: the tie of the base of Core 397-U1587C-29X to the top of Core 397-U1587A-29X that was adjusted by ~55 cm in the final composite relative to the shipboard splice. Reexamination of all shipboard data identified one splice interval that was not covered by XRF scanning: the tie of the base of Core 397-U1587A-21X to the top of Core 397-U1587B-21X. The splice here was based on the best tie point available using the combination of MS, NGR, and L* as constraints. Of these, the NGR data provide the most robust hole-to-hole correlation tool, and we selected a tie point that results in a gap of 36 cm in XRF coverage (Figure **F5**) and a splice with 95 cm from Core 397-U1587B-21X added in comparison to the shipboard composite. In comparison to the spliced section reported in **Hodell et al.** (2024b), we retain an identical number of tie points (113) but adjusted the splice and affine tables based on the XRF Ca/Ti ratios as the primary correlation metric.

3. Results

3.1. XRF measurements of Site U1587 Pliocene and Quaternary sections

A total of 67,226 measurements were acquired at 1 cm intervals using both low (10 kV) and medium (30 kV) energy settings on all cores included in the spliced section spanning from the seafloor to 400 m CCSF. Of these, only 892 measurements (1.33%) recorded positive Ar counts

and were excluded from the data set presented in this report. Three core sections from Hole U1587B (Sections 397-U1587B-23X-1A, 23X-3A, and 38X-4A) and one from Hole U1587C (Section 397-U1587C-39X-2A) were reconditioned and rescanned because of an initially high proportion of scan steps with positive Ar counts. The XRF core measurements provide a high-resolution record of semiquantitative element data from the base of the Pliocene through Holocene sediments cored at Site U1587. The average sedimentation rate across this section is ~10 cm/ky (**Hodell et al.**, 2024b). Therefore, a 1 cm measurement interval corresponds to a temporal resolution of approximately 100 hundred years between data points, although the actual resolution is more likely on the order of hundreds of years because of bioturbation but nevertheless high enough to detect millennial events. Bioturbation is common in the Site U1587 cores in the form of burrows and trace fossils, but there is no evidence that it affected the integrity and cyclicity of the sediment physical properties (e.g., NGR, MS, or color reflectance) (**Hodell et al.**, 2024b).

Downhole distributions of selected elements commonly used to distinguish between biogenic and lithogenic sources (Peterson and Schimmenti, 2020) are presented on the composite depth scale in Figures **F6** and **F7**. The profiles of calcium (Ca), strontium (Sr), and bromine (Br) (Figure **F6**) primarily reflect biogenic sediment components. Ca and Sr, both proxies for the abundance of calcareous microfossils, exhibit a strong positive correlation throughout the record (r = 0.98; Table **T1**). In contrast, Br concentrations increase gradually from the base of the record to ~50 m CCSF, fol-

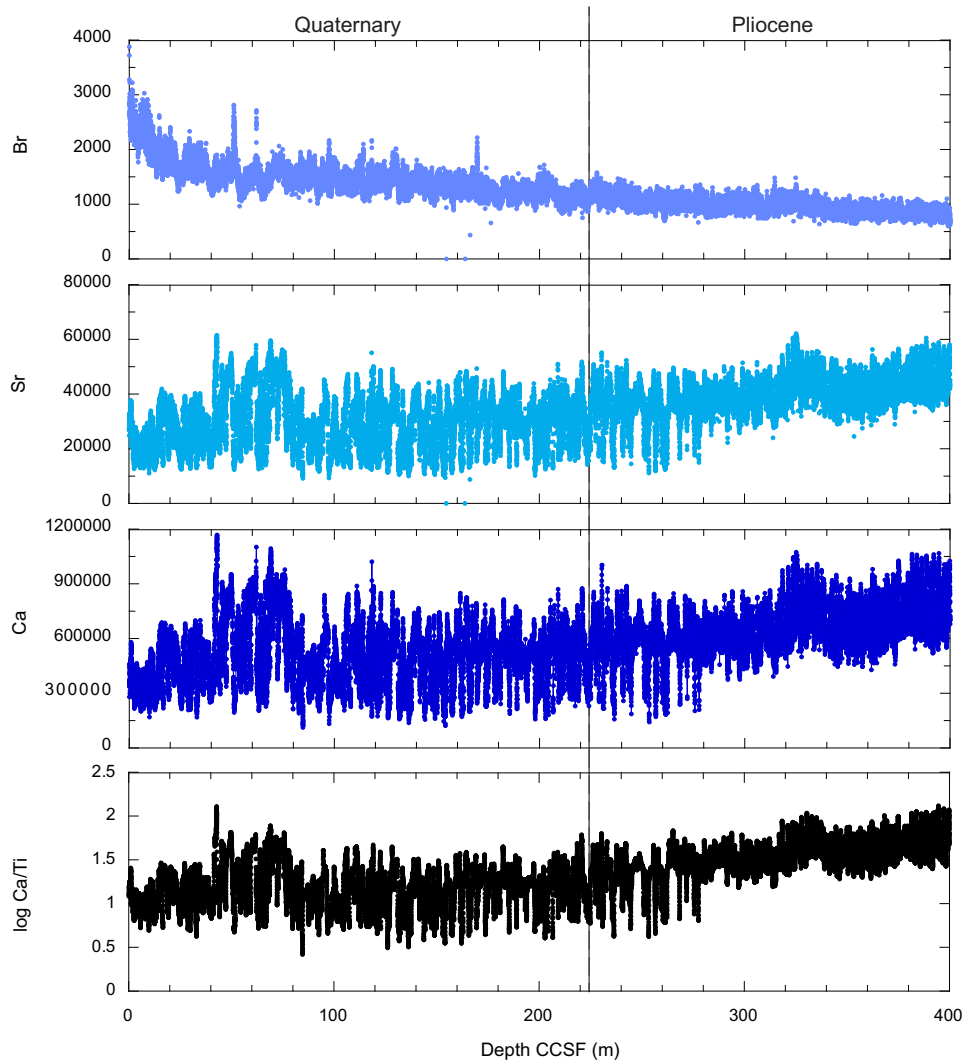

Figure F6. Pliocene through Quaternary trends in XRF counts of biogenic elements and log(Ca/Ti) record on Site U1587 composite depth scale. Ca counts were measured at 10 kV. Br and Sr counts were measured at 30 kV. Log(Ca/Ti) was used to refine Site U1587 splice.

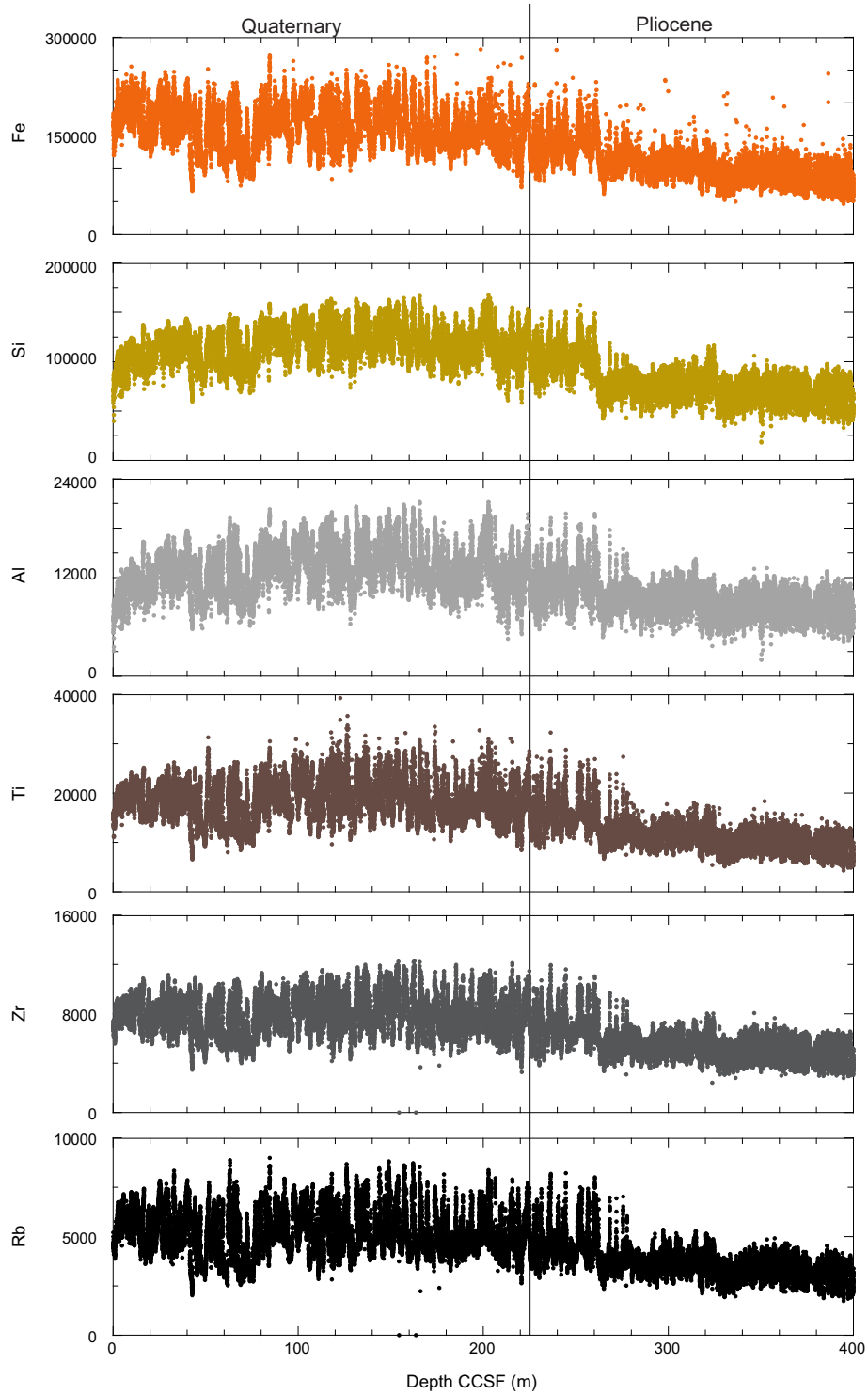

Figure F7. Pliocene through Quaternary trends in XRF counts for lithogenic elements on Site U1587 composite depth scale. Fe, Al, Si, and Ti counts were measured at 10 kV. Zr and Rb counts were measured at 30 kV.

Table T1. Correlation coefficients and covariance values between biogenic and lithogenic elements, Site U1587. **Download table in CSV format.**

lowed by a sharper rise toward the seafloor. As a proxy for total organic carbon (TOC) in marine sediments (Ziegler et al., 2008; Seki et al., 2019; Peterson and Schimmenti, 2020), Br trends suggest increasing organic matter accumulation upcore.

Terrigenous elements aluminum (Al), iron (Fe), titanium (Ti), silicon (Si), zirconium (Zr), and rubidium (Rb) are shown in Figure **F7**. These elements display similar downhole patterns and strong interelement correlations, indicating a shared lithogenic origin. Notably, their concentrations are lower in the Pliocene and increase markedly in both intensity and variability through the Pleistocene.

Crossplots of biogenic and terrigenous element pairs (Figure **F8**) further illustrate the relationships between these sedimentary components and support the distinction between their respective sources.

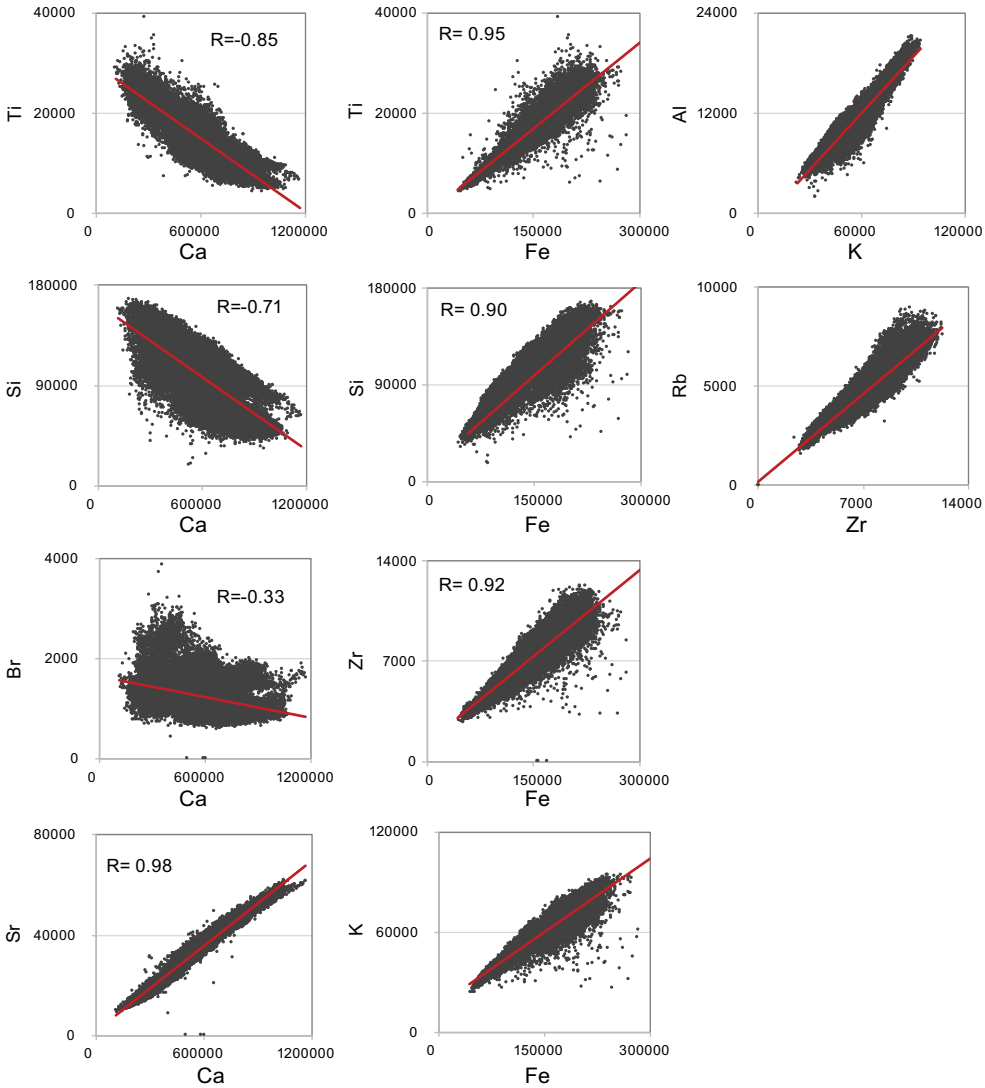

Figure F8. Crossplots of elements typically associated with biogenic (Ca, Sr, and Br) and detrital (Fe, Al, Si, Ti, Zr, and Rb) inputs to marine sediments, Site U1587. Linear Pearson correlation coefficients (*R*) are displayed for each plot. See Table T1 for correlation coefficients and covariance values between elements. Ca, Fe, Al, Si, and Ti counts were measured at 10 kV. Sr, Br, Zr, and Rb counts were measured at 30 kV.

Table T2. Affine table, Site U1587 (version 7). **Download table in CSV format.**

Table T3. Splice table, Site U1587 (version 5). **Download table in CSV format.**

Table T4. XRF data (10 kV) along the splice, Site U1587. **Download table in CSV format.**

Table T5. XRF data (30 kV) along the splice, Site U1587. **Download table in CSV format.**

3.2. Stratigraphic correlation

A shipboard splice was constructed to 595 m CCSF by correlating physical properties across the three holes (U1587A–U1587C) (**Hodell et al.**, 2024b). For this report, we revised the original affine and splice tables using high-resolution Ca/Ti data obtained from XRF core scanning. We retained an identical number of tie points (113) but adjusted the splice and affine tables. Only one tie point between Samples 397-U1587B-21X-6, 115 cm, and 22X-1, 99 cm, was revised using NGR to fill in a gap in XRF scanning. Every effort was made to adhere as closely as possible to the original sampling splice to ensure that discrete samples will fall on the revised splice, minimizing potential gaps. The updated affine and splice tables for Site U1587 are provided in Tables **T2** (affine-7) and **T3** (splice-5) and are also available from the IODP Laboratory Information Management System (LIMS) at **https://web.iodp.tamu.edu/LORE**, where they can be used to readily download shipboard data on the splice (CCSF) depth scale.

3.3. XRF data availability

The 10 and 30 kV XRF data, measured in counts per second, for all sections included in the Pliocene through Holocene spliced interval at Site U1587 are provided in Tables **T4** (10 kV) and **T5** (30 kV). The data are also permanently archived in LIMS and at Zenodo (**https://zenodo.org/communities/iodp**), where the raw dataset can be downloaded by hole on the CSF-A or CCSF-A depth scales.

4. Acknowledgments

The IODP programmatic XRF measurements were supported by the National Science Foundation (NSF). The acquisition of additional measurements required to complete the XRF scanning of the Site U1587 spliced record was possible thanks to financial contributions from C.A. Alvarez Zarikian, T.D. Herbert, L. Nana Yobo, J.F. McManus, M. Alonso-Garcia, and J.-A. Flores. We thank the Gulf Coast Core Repository staff at Texas A&M University for curating, storing, and providing the cores for analyses after Expedition 397. C.A. Alvarez Zarikian acknowledges funding support from NSF award OCE-1326927. T.D. Herbert and L. Nana Yobo acknowledge funding support from NSF award OCE-1450528. J.F. McManus acknowledges funding support from NSF awards EAR 24-20482 and OCE-24-42513. M. Alonso-Garcia and J.-A. Flores acknowledge funding support from the Spanish MICCIN through the project PICTURE (PID2021-128322NB-I00).

References

Abrantes, F., Hodell, D.A., Alvarez Zarikian, C.A., Brooks, H.L., Clark, W.B., Dauchy-Tric, L.F.B., dos Santos Rocha, V., Flores, J.-A., Herbert, T.D., Hines, S.K.V., Huang, H.-H.M., Ikeda, H., Kaboth-Bahr, S., Kuroda, J., Link, J.M., McManus, J.F., Mitsunaga, B.A., Nana Yobo, L., Pallone, C.T., Pang, X., Peral, M.Y., Salgueiro, E., Sanchez, S., Verma, K., Wu, J., Xuan, C., and Yu, J., 2024. Expedition 397 methods. In Hodell, D.A., Abrantes, F., Alvarez Zarikian, C.A., and the Expedition 397 Scientists, Iberian Margin Paleoclimate. Proceedings of the International Ocean Discovery Program, 397: College Station, TX (International Ocean Discovery Program). **https://doi.org/10.14379/iodp.proc.397.102.2024**

Abrantes, F., Magalhães, V., Hodell, D.A., Herbert, T.D., Alonso-Garcia, M., Castaño, M., Ferreira, F., Freitas, M., Gebara, L., Gil, I., Gonzáles-Martín, M., Lopes, A., Lopes, C., Matos, L., Mega, A., Molina, G., Naughton, F., Oliveira,

D., Rebotim, A., Rodrigues, T., Salgueiro, E., Santana, A., Treyos-Tamayo, R., Alvarez Zarikian, C.A., and the Expedition 397 Scientists, 2025. Data report: an improved splice using XRF data, IODP Expedition 397 Site U1586. In Hodell, D.A., Abrantes, F., Alvarez Zarikian, C.A., and the Expedition 397 Scientists, Iberian Margin Paleoclimate. Proceedings of the International Ocean Discovery Program, 397: College Station, TX (International Ocean Discovery Program). **https://doi.org/10.14379/iodp.proc.397.202.2025**

Bahr, A., Jiménez-Espejo, F.J., Kolasinac, N., Grunert, P., Hernández-Molina, F.J., Röhl, U., Voelker, A.H.L., Escutia, C., Stow, D.A.V., Hodell, D., and Alvarez-Zarikian, C.A., 2014. Deciphering bottom current velocity and paleoclimate signals from contourite deposits in the Gulf of Cádiz during the last 140 kyr: an inorganic geochemical approach. Geochemistry, Geophysics, Geosystems, 15(8):3145–3160. **https://doi.org/10.1002/2014GC005356**

Balsam, W.L., Deaton, B.C., and Damuth, J.E., 1999. Evaluating optical lightness as a proxy for carbonate content in marine sediment cores. Marine Geology, 161(2):141–153. **https://doi.org/10.1016/S0025-3227(99)00037-7**

Croudace, I.W., and Rothwell, R.G. (Eds.), 2015. Micro-XRF Studies of Sediment Cores: Applications of a Non-destructive Tool for the Environmental Sciences: Dordrecht, Netherlands (Springer). **https://doi.org/10.1007/978-94-017-9849-5**

Flecker, R., Ducassou, E., Williams, T., and the Expedition 401 Scientists, 2024. Expedition 401 Preliminary Report: Mediterranean–Atlantic Gateway Exchange. International Ocean Discovery Program. **https://doi.org/10.14379/iodp.pr.401.2024**

Hodell, D., Lourens, L., Crowhurst, S., Konijnendijk, T., Tjallingii, R., Jiménez-Espejo, F., Skinner, L., Tzedakis, P.C., and the Shackleton Site Project Members, 2015. A reference time scale for Site U1385 (Shackleton Site) on the SW Iberian Margin. Global and Planetary Change, 133:49–64. **https://doi.org/10.1016/j.gloplacha.2015.07.002**

Hodell, D.A., Abrantes, F., Alvarez Zarikian, C.A., Herbert, T.D., Du, M., Crowhurst, S.J., Mleneck-Vautravers, M., Rolfe, J.E., Chen, X., Brooks, H.L., Clark, W.B., Dauchy-Tric, L.F.B., dos Santos Rocha, V., Flores, J.-A., Hines, S.K.V., Huang, H.-H.M., Ikeda, H., Kaboth-Bahr, S., Kuroda, J., Link, J.M., McManus, J.F., Mitsunaga, B.A., Nana Yobo, L., Pallone, C.T., Pang, X., Péral, M.Y., Salgueiro, E., Sanchez, S., Verma, K., Wu, J., Xuan, C., Yu, J., Haygood, L.A., Liebrand, D., Magalhães, V., Alonso-Garcia, M., Castaño, M., Ferreira, F., Freitas, M., Gebara Cordeiro, L., Gil, I., González-Martín, M., Lopes, A., Lopes, C., Margari, V., Martín-García, L., Matos, L., Mega, A., Molina, G., Naughton, F., Oliveira, D., Rebotim, A., Rodrigues, T., Santana, A., Trejos-Tamayo, R., and Tzedakis, P.C, in press. Onset of millennial climate variability with the intensification of Northern Hemisphere glaciation. Science.

Hodell, D.A., Abrantes, F., Alvarez Zarikian, C.A., Brooks, H.L., Clark, W.B., Dauchy-Tric, L.F.B., dos Santos Rocha, V., Flores, J.-A., Herbert, T.D., Hines, S.K.V., Huang, H.-H.M., Ikeda, H., Kaboth-Bahr, S., Kuroda, J., Link, J.M., McManus, J.F., Mitsunaga, B.A., Nana Yobo, L., Pallone, C.T., Pang, X., Peral, M.Y., Salgueiro, E., Sanchez, S., Verma, K., Wu, J., Xuan, C., and Yu, J., 2024a. Expedition 397 summary. In Hodell, D.A., Abrantes, F., Alvarez Zarikian, C.A., and the Expedition 397 Scientists, Iberian Margin Paleoclimate. Proceedings of the International Ocean Discovery Program, 397: College Station, TX (International Ocean Discovery Program). **https://doi.org/10.14379/iodp.proc.397.101.2024**

Hodell, D.A., Abrantes, F., Alvarez Zarikian, C.A., Brooks, H.L., Clark, W.B., Dauchy-Tric, L.F.B., dos Santos Rocha, V., Flores, J.-A., Herbert, T.D., Hines, S.K.V., Huang, H.-H.M., Ikeda, H., Kaboth-Bahr, S., Kuroda, J., Link, J.M., McManus, J.F., Mitsunaga, B.A., Nana Yobo, L., Pallone, C.T., Pang, X., Peral, M.Y., Salgueiro, E., Sanchez, S., Verma, K., Wu, J., Xuan, C., and Yu, J., 2024b. Site U1587. In Hodell, D.A., Abrantes, F., Alvarez Zarikian, C.A., and the Expedition 397 Scientists, Iberian Margin Paleoclimate. Proceedings of the International Ocean Discovery Program, 397: College Station, TX (International Ocean Discovery Program). **https://doi.org/10.14379/iodp.proc.397.104.2024**

Hodell, D.A., Crowhurst, S.J., Mleneck-Vautravers, M.J., Rolfe, J.E., Du, M., Herbert, T.D., Huang, H.-H.M., Abrantes, F., Alvarez Zarikian, C.A., and the Expedition 397 Scientists, 2026. Data report: composite section and chronology of IODP Sites 339-U1385 and 397-U1385 based on postcruise XRF analysis. In Hodell, D.A., Abrantes, F., Alvarez Zarikian, C.A., and the Expedition 397 Scientists, Iberian Margin Paleoclimate. Proceedings of the International Ocean Discovery Program, 397: College Station, TX (International Ocean Discovery Program). **https://doi.org/10.14379/iodp.proc.397.204.2026**

Hodell, D., Crowhurst, S., Skinner, L., Tzedakis, P.C., Margari, V., Channell, J.E.T., Kamenov, G., Maclachlan, S., and Rothwell, G., 2013. Response of Iberian margin sediments to orbital and suborbital forcing over the past 420 ka. Paleoceanography and Paleoclimatology, 28(1):185–199. **https://doi.org/10.1002/palo.20017**

Jenkins, W.J., Smethie, W.M., Boyle, E.A., and Cutter, G.A., 2015. Water mass analysis for the U.S. GEOTRACES (GA03) North Atlantic sections. Deep Sea Research, Part II: Topical Studies in Oceanography, 116:6–20. **https://doi.org/10.1016/j.dsr2.2014.11.018**

Lamy, F., Winckler, G., Arz, H.W., Farmer, J.R., Gottschalk, J., Lembke-Jene, L., Middleton, J.L., van der Does, M., Tiedemann, R., Alvarez Zarikian, C., Basak, C., Brombacher, A., Dumm, L., Esper, O.M., Herbert, L.C., Iwasaki, S., Kreps, G., Lawson, V.J., Lo, L., Malinverno, E., Martinez-Garcia, A., Michel, E., Moretti, S., Moy, C.M., Ravelo, A.C., Riesselman, C.R., Saavedra-Pellitero, M., Sadatzki, H., Seo, I., Singh, R.K., Smith, R.A., Souza, A.L., Stoner, J.S., Toyos, M., de Oliveira, I.M.V.P., Wan, S., Wu, S., and Zhao, X., 2024. Five million years of Antarctic Circumpolar Current strength variability. Nature, 627(8005):789–796. **https://doi.org/10.1038/s41586-024-07143-3**

Peterson, L.C., Haug, G.H., Hughen, K.A., and Röhl, U., 2000. Rapid changes in the hydrologic cycle of the Tropical Atlantic during the Last Glacial. Science, 290(5498):1947–1951. **https://doi.org/10.1126/science.290.5498.1947**

Peterson, L.C., and Schimmenti, D.E., 2020. Data report: X-ray fluorescence scanning of Site U1427, Yamato Basin, Expedition 346. In Tada, R., Murray, R.W., Alvarez Zarikian, C.A., and the Expedition 346 Scientists, Proceedings of the Integrated Ocean Drilling Program. 346: College Station, TX (Integrated Ocean Drilling Program). **https://doi.org/10.2204/iodp.proc.346.206.2020**

Raad, F., Standring, P., Le Ber, E., Blättler, C., Billy, I., Chin, S., Teixeira, M., Feakins, S.J., Li, Z., Mulligan, M., Noto, D., Stine, J., Xu, X., Yeon, J., Yousfi, Z.M., Zhang, Y., Flecker, R., Ducassou, E., Williams, T., and the Expedition 401

Scientists, 2026. Data report: X-ray fluorescence scanning of sediment cores, IODP Expedition 401 Site U1385, southwest Iberian margin (Portugal). In Flecker, R., Ducassou, E., Williams, T., and the Expedition 401 Scientists, Mediterranean–Atlantic Gateway Exchange. Proceedings of the International Ocean Discovery Program, 401: College Station, TX (International Ocean Discovery Program). **https://doi.org/10.14379/iodp.proc.401.202.2026**

Richter, T.O., van der Gaast, S., Koster, B., Vaars, A., Gieles, R., de Stigter, H.C., De Haas, H., and van Weering, T.C.E., 2006. The Avaatech XRF Core Scanner: technical description and applications to NE Atlantic sediments. In Rothwell, R.G., New Techniques in Sediment Core Analysis. Geological Society Special Publication, 267: 39–50. **https://doi.org/10.1144/GSL.SP.2006.267.01.03**

Seki, A., Tada, R., Kurokawa, S., and Murayama, M., 2019. High-resolution Quaternary record of marine organic carbon content in the hemipelagic sediments of the Japan Sea from bromine counts measured by XRF core scanner. Progress in Earth and Planetary Science, 6(1):1. **https://doi.org/10.1186/s40645-018-0244-z**

Tjallingii, R., Röhl, U., Kölling, M., and Bickert, T., 2007. Influence of the water content on X-ray fluorescence core-scanning measurements in soft marine sediments. Geochemistry, Geophysics, Geosystems, 8(2):Q02004. **https://doi.org/10.1029/2006GC001393**

Wu, L., Wilson, D.J., Wang, R., Yin, X., Chen, Z., Xiao, W., and Huang, M., 2020. Evaluating Zr/Rb ratio from XRF scanning as an indicator of grain-size variations of glaciomarine sediments in the Southern Ocean. Geochemistry, Geophysics, Geosystems, 21(11):e2020GC009350. **https://doi.org/10.1029/2020GC009350**

Ziegler, M., Jilbert, T., de Lange, G.J., Lourens, L.J., and Reichart, G.-J., 2008. Bromine counts from XRF scanning as an estimate of the marine organic carbon content of sediment cores. Geochemistry, Geophysics, Geosystems, 9(5). **https://doi.org/10.1029/2007GC001932**